Study of the Interaction of Pollutant Nitro Polycyclic Aromatic Hydrocarbons with Different Metallic Surfaces by Surface-Enhanced Vibrational Spectroscopy (SERS and SEIR)

E. A. Carrasco F., M. Campos-Vallette,[†] P. Leyton,[†] G. Diaz F.,[‡] R. E. Clavijo,[†] J. V. García-Ramos,[§] N. Inostroza,[†] C. Domingo,[§] S. Sanchez-Cortes,*[,§] and R. Koch[#]

University of Chile, Faculty of Sciences, PO Box 653, Santiago, Chile, University of Playa Ancha, Faculty of Science, PO Box 34, V. Valparaiso, Chile, Consejo Superior de Investigaciones Científicas (CSIC), Instituto de Estructura de la Materia, Serrano 121, Madrid 28006, Spain, and Department of Chemistry, University of Oldenburg, D-26129 Oldenburg, Germany

Received: May 7, 2003; In Final Form: September 10, 2003

In this work, we have applied surface-enhanced Raman scattering (SERS) and surface-enhanced infrared spectroscopy (SEIR) to study the interaction of nitro polycyclic aromatic hydrocarbons (NPAHs) with metal surfaces. The nitro group confers the polycyclic aromatic hydrocarbons (PAHs) moiety additional electronic and structural characteristics which verify NPAHs−surface interactions. SERS and SEIR spectra suggest that the NPAHs 1-nitropyrene (1NP) and 2-nitrofluorene (2NF) at concentrations of $<10^{-6}$ M (∼200 ppb) interact with metal surfaces through the nitro group, adopting a perpendicular orientation onto the surface. In both cases, the interaction seems to occur through the O atoms of the nitro groups, which are coplanar to the PAHs fragment. The most efficient interaction was obtained using silver metal colloidal surfaces. The mechanism of interaction with the metal surface is related to the structure of NPAHs: although a monodentate interaction is deduced in the case of 1NP, a bidentate one seems to occur in the case of 2NF. To complete this study, theoretical Raman vibrational spectra of both free 2NF and their complexes with silver metal clusters were obtained using the local spin density approximation (LSDA) methods with the LAN12DZ basis set. The theoretical calculations were compared to the experimental results, obtaining a good agreement with the SERS and SEIR data.

Introduction

Nitro polycyclic aromatic hydrocarbons (NPAHs) are derivatives of polycyclic aromatic hydrocarbons (PAHs), which contain two or more fused aromatic rings that are composed of C and H atoms. NPAHs occur in the environment as a mixture with parent PAHs and hundreds of other organic compounds. NPAHs are usually present in much smaller quantities than PAHs.[1]

NPAHs in the environment either occur in the vapor phase or are adsorbed onto particulate matter, and they are insoluble or sparingly soluble in water but are primarily soluble in organic solvents. These nitro derivatives originate from PAHs via nitration during combustion processes (e.g., in vehicle exhaust, particularly diesel, but also gasoline and aircraft emissions; industrial emissions; domestic residential heating/cooking; wood burning) or via reaction with nitrogen dioxide (NO_2).[1−5] The distribution of NPAH isomers in samples of ambient air has been found to be significantly different from that in direct emissions from combustion. The most abundant nitro isomers of pyrene and fluorene observed in diesel exhaust are 1-nitropyrene (1NP) and 2-nitrofluorene (2NF)[1] (Figure 1), which are the subject of the present work.

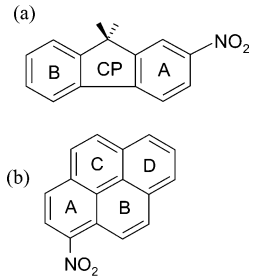

Figure 1. Molecular structure of (a) 2-nitrofluorene (2NF) and (b) 1-nitropyrene (1NP).

NPAHs have been reported to be carcinogenous compounds,[6] with a toxic activity that could be higher than the parent PAHs compounds.[1] NPAHs can form adducts with DNA, inducing mutations in GC-rich sequences.[6−8] In addition, they can also interact with proteins. In the last case, the interaction has been reported to occur through the heme group of proteins, rather than with the peptidic group.[9]

The environmental importance of NPAHs, in relation to human health, leads us to develop new detection devices that are based on surface-enhanced vibrational spectroscopy (SEVS), toward the design and implementation of optical sensors based on SEVS.

The vibrational (IR and Raman) spectra of PAHs have been largely reported;[10−17] however, vibrational studies on NPAHs are comparatively less abundant. Juchnovski and Andreev[18] reported the IR spectra of 38 nitro compounds, including some

* Author to whom correspondence should be addressed. E-mail: imts158@iem.cfmac.csic.es.
[†] University of Chile.
[‡] University of Playa Ancha.
[§] Consejo Superior de Investigaciones Científicas (CSIC), Instituto de Estructura de la Materia.
[#] University of Oldenburg.

10.1021/jp035242a CCC: $25.00
Published on Web 10/18/2003

NPAHs. In a Raman study, Li et al.[10] determined the orientation of the nitro group in several NPAHs such as 2-nitroanthracene (**I**), 7-nitrobenzo[*a*]anthracene (**II**), 6-nitrochrysene (**III**), 1NP (**IV**), 6-nitrobenzo[*a*]pyrene (**V**), and 6-nitro-7,8,9,10-tetrahydrobenzene (**VI**). Raman depolarization ratio data of compounds in solution indicate that the nitro group is in-plane with the PAHs plane in **I**, **III**, and **IV**, whereas NO_2 is perpendicular to the molecular plane in **II**, **V**, and **VI**. X-ray data indicate that the substituent is almost perpendicular in 9-nitroantracene.[19] In this work, we report the ^{1}H NMR data for 2NF, which shows that signals that correspond to the fluorene aromatic H atoms shift to low field; this leads us to propose that the NO_2 fragment is coplanar to the PAHs moiety. The analysis of conformational data of the nitrocompounds is interesting, taking into account their different structural possibilities of interaction with surfaces.

Surface-enhanced vibrational spectroscopy (SEVS) currently is an active area with a broad range of analytical applications. In particular, surface-enhanced infrared and surface-enhanced Raman scattering spectroscopies (SEIR and SERS, respectively) have attracted much attention from the first observation of both phenomena.[20,21] Although these techniques are based on the enormous enhancement of the electromagnetic field occurring in the vicinity of metallic nanoparticles, mainly of silver and gold, chemical contributions to the total enhancement in both effects, SEIR and SERS, has been also suggested.[22,23]

SERS and SEIR have been the basis for the application of the vibrational spectroscopy to the analysis of molecular systems in the range of nanograms to femtograms. They currently are recognized as useful analytical techniques, because of their applicability in the surface chemistry to determine the identity and most probable orientation of molecules adsorbed onto a surface.[24,25] The electromagnetic enhancement of a signal in SERS strongly depends on different physical and physical chemistry characteristics of the surface. Recent investigations that involve silver and gold metals were oriented to obtain the most-efficient amplifying surfaces.[26]

In the application of such surface analytical techniques, it is necessary to consider the fact that each analyte requires a certain type of substrate. Determination of the best substrate is an important initial step in the design of possible sensor systems that are based on SEVS spectroscopy. Vo-Dinh et al. has pioneered the analysis of PAH by the application of several detection techniques[27]—particularly, the SERS technique—to the analysis of PAHs.[28] SERS of some NPAHs (1NP, 9-nitroanthracene, 2-nitronaphthalene, and 2NF) has been previously reported by Enlow et al.,[29] where different silver substrates, with respect to those investigated in the present work, were used, and the viability of the latter surfaces was investigated from an analytical point of view. However, in the work by Enlow et al., no interpretation about the interaction mechanism and the orientation of the adsorbates was made. We understand that this interpretation could be helpful in the determination of new substrates for the analytical detection of these important chemical pollutants.

With respect to the metal−adsorbate interaction, it is of interest to develop theoretical calculations based on molecular models that involve the adsorbate molecules and metal cluster, for comparison with the experimental results. In this work, density functional theory (DFT) was applied to simulate such systems. Works by Scott and Radom[30] and Wong[31] showed that DFT consistently predicts harmonic vibrational frequencies in better agreement with observed fundamentals than conventional ab initio methods at a much lower cost. Comparison of observed fundamental with computed harmonics using the 6-31G(d) basis set gave scaling factors of 0.9833 for S-VWN, 0.9945 for B-LYP, and 0.9614 for B3-LYP, whereas scale factors for conventional ab initio methods were 0.9427 and 0.9537 for MP2 and QCISD, respectively.[30,31]

The purpose of the present work was multiple:

(1) To study the adsorption of the NPAHs 1-nitropyrene (1NP) and 2-nitrofluorene (2NF) (Figure 1) on metal surfaces prepared by different procedures: silver- and gold-metal integrating substrates with different preparation procedures (colloids and evaporated films) were used to determine the best surface for the study of these molecules;

(2) To identify small amounts of the aforementioned NPAHs, using SEVS spectroscopy;

(3) To deduce the mechanism of the adsorbate−substrate interaction;

(4) To complete the vibrational assignment of NPAHs based on their IR and Raman spectra and the vibrational assignment of the PAHs compounds pyrene and fluorene; and finally

(5) To perform DFT theoretical calculations regarding the energetics of the adsorbate−substrate interaction for an approximate molecular model.

Experimental Section

Preparation of the Metal Surfaces and Samples for SEVS Spectroscopy. 2NF and 1NP were purchased from Aldrich and Merck, respectively, and used as received. Solutions of these compounds in ethanol (99%) were prepared to a final concentration of 10^{-5} M. For the measurements in silver colloids and, eventually, gold colloids, 50 μL of the solutions were added to 500 μL of silver colloid. For the measurements on gold-metal island films, aliquots of those ethanol solutions were also deposited onto the metal surfaces. In the SERS experiments, samples with low and high concentrations were prepared by depositing different solution volumes to the metal film in the case of 1NP, and by washing samples with a high initial concentration with ethanol, in the case of 2NF. All the spectra were registered after complete solvent evaporation.

Silver colloids were prepared using citrate[32] and borohydride[33] as reducing agents. Gold island surfaces for the SERS and SEIR experiments were obtained via the sublimation of gold onto germanium plates, according to the procedure described elsewhere.[34] The last material was used as a substrate for the gold evaporation, because of the higher IR transmission properties of germanium between 800 and 400 cm^{-1}.

The final NPHAs concentration was 10^{-6} M in the metal colloids. A small solution volume ($\sim 1.6 \times 10^8$ μm^3) was analyzed by the laser beam to obtain the Raman spectra. Thus, the amount of analyte studied in each experiment was ~400 pg.

In the case of metal island films, the sensitivity is much higher, because a small surface area was studied by micro-Raman analysis. Assuming that the applied aliquot (10^{-5} M) reached a whole surface of $\sim 10^8$ μm^2, and that the analyzed surface is 2 μm^2 (when using a 100× objective in the micro-Raman analysis), we have calculated that the total analyzed NPAHs is $\sim 10^{-3}$ pg. This means that the sensitivity of the micro Raman analysis is 10^5 times greater than the colloidal samples. The analyte was spread uniformly on the metal surface, as deduced from the similar Raman intensity registered in different points.

Instrumentation. The FTIR spectra in the region of 4000−450 cm^{-1} were registered using a Perkin−Elmer Series 2000 apparatus. This spectrometer operates with a deuterated triglycine sulfate (DTGS) detector. Spectra were registered with a

resolution of 4 cm^{-1}. Transmission SEIR spectra were registered in a Bruker model IFS 66 instrument that had a DTGS detector. The spectra resolution was 8 cm^{-1}, and 100 scans were obtained from each sample.

Fourier transform−Raman spectra of the solid compounds were obtained through the use of a Bruker model RFS 100/S instrument, using the line at 1064 nm, which was provided by a Nd:YAG laser and a germanium detector that was cooled by liquid nitrogen. The resolution was set to 4 cm^{-1}, and the 180° geometry was used. The output laser power was 50−100 mW. The solid samples were placed in a brass holder. Up to 1000 scans were accumulated.

The SERS spectra at 785 nm were measured with a Renishaw Raman microscope (System RM1000) equipped with a diode laser, a Leica microscope, and an electrically refrigerated CCD camera. The spectra shown here were obtained using a 100× objective. The output laser power was in the range of 1.0−3.0 mW, and the spectral resolution was 4 cm^{-1}.

The SERS spectra at 514.5 nm were obtained in a Jobin−Yvon model U-1000 spectrophotometer, using an Spectra Physics model 165 argon-ion laser. The resolution was set to 4 cm^{-1}, and a 90° geometry was used to record the data. The laser power at the sample was fixed at 40 mW. Experiments were performed by taking one scan with a step size of 1 cm^{-1} and an integration time of 1 s. The samples for SERS measurements in this Raman spectrophotometer were placed in 1-mm-diameter glass capillaries.

UV−visible spectra were recorded using Karl−Zeiss DMR model 22 and Varian Cary model 1E equipment.

Finally, ^1H NMR spectra were recorded with a Bruker model AMX-300 apparatus.

Calculations

The calculations were performed only for 2NF, supposing a bidentate interaction of this molecule through both O atoms with two Ag atoms. For 1NP, we are performing another calculation, which assumes a monodentate interaction. These different calculations are justified by the model interactions deduced from the SEVS spectra, which will be shown below.

Methodology. After optimization of the molecular geometry at the same level of theory, DFT harmonic frequencies were computed, using the S-VWN exchange-correlation functional, which is also known as the local spin density approximation (LSDA). It consists of Slater's local spin density exchange functional[35] and the correlation functional by Vosko, Wilk, and Nusair.[36] The basis set used throughout is the LANL2DZ, which corresponds to the D95 basis set on first-row atoms and the Los Alamos ECP plus DZ basis set on the Ag atom.[37] Scaling of the harmonic frequencies due to the anharmonicity of the molecules is described in the text. The DFT calculations were performed using the Gaussian 98 program package.[38]

Molecular Models. Two different 2NF−metal complexes were used for the calculations: (a) $2NF/Ag_2$, where each Ag atom is attached to each O atom of the 2NF nitro group; and (b) $2NF/Ag_{10}$, where the 2 central Ag atoms that are interacting with each O atom of the 2NF nitro group are surrounded by 8 Ag atoms, so that a plane of 10 atoms is formed (see inset drawings in Figure 8, presented later in this work). In both cases, the 2NF molecule was placed perpendicularly, with the O atoms of the nitro group in contact with the two central metal atoms, and the entire system was optimized.

Results and Discussion

Infrared and Raman Assignment. The band assignments for 1NP and 2NF were performed by considering our spectral data for the precursors pyrene and fluorene, the tables of characteristic group frequencies,[39−41] and the proposed spectral assignments for related compounds. [10,42,43]

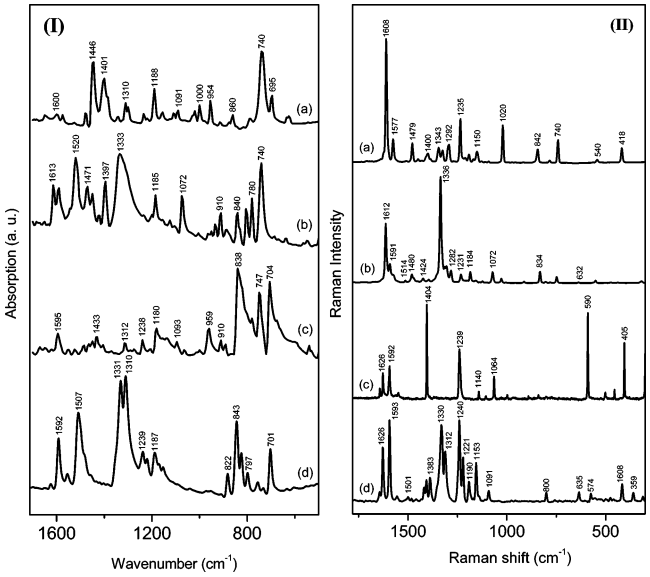

Figure 2. (I) Infrared and (II) Raman spectra of various materials. Panel I shows IR spectra for pyrene (spectrum a), 1NP (spectrum b), fluorene (spectrum c), and 2NF (spectrum d) in the region of 1750−450 cm^{-1}. Panel II shows Raman spectra of pyrene (1064 nm; spectrum a), 1NP (785 nm; spectrum b), fluorene (785 nm; spectrum c), and 2NF (785 nm; spectrum d) in solid state.

Comparison of the spectra of the NPAHs with those corresponding to the relative PAHs allowed us to (a) identify the nitro fundamental bands and (b) distinguish vibrations close and far from the nitro substitution site. The IR spectra (panel I in Figure 2 and Table 1) clearly display the NO_2 bands that correspond to the asymmetric and symmetric $\nu(NO_2)$ modes at 1520 and 1333 cm^{-1} in 2NF (spectrum b in panel I of Figure 2), and at 1507 and 1331/1310 cm^{-1} in 1NP (spectrum d in panel I of Figure 2). The asymmetry, wideness, and relative high intensity of the symmetric $\nu_s(NO_2)$ band suggest the coexistence of another mode that is probably related to the νCN vibration, as observed in *N*-benzylideneanilines.[44,45] The Raman spectra of 2NF and 1NP (panel II in Figure 2 and Table 1) display the characteristic NO_2 bands at similar wavenumbers as in the IR spectra, with the difference being that the asymmetric mode band is much weaker. The bands corresponding to the NO_2 deformation mode ($\delta(NO_2)$) are observed in Raman analysis at 635 and 632 cm^{-1} in 1NP and 2NF, respectively. Because of the low symmetry of the nitrocompounds, most of the bands are observed in both the IR and Raman spectra.

The ν(CC) aromatic modes are normally observed between 1700 and 1400 cm^{-1}. Generally, a frequency shift to higher energy by nitro substitution is observed, because of a π electronic redistribution imposed by the electron acceptor characteristics of the NO_2 group. The most important changes should be ascribed to spectral modes that correspond to the CC bonds closest to the nitro fragment. Spectral shifts to lower energy should correspond to modes that involve CC bonds far from the substitution site. For instance, the Raman band of 1NP at 1404 cm^{-1} is strongly affected by the nitro substitution, suggesting that this mode may correspond to the A-ring (see Figure 1), where the nitro group is attached.

The aromatic in-plane CH deformation modes (δ(CH)), coupled with ν(CC) vibrations, are expected to appear in the 1250−1000 cm^{-1} region. The IR bands observed at 1022 and

TABLE 1: Main IR and Raman Wavenumbers and Assignments of Fluorene, Pyrene, and Their Nitro Derivatives

wavenumber[a] (cm^{-1})								
fluorene		2NF		pyrene		1NP		
IR	Raman	IR	Raman	IR	Raman	IR	Raman	assignment[b]
1648w		1648vw			1641w		1645w	ν(CC)
1600w	1608s	1613m	1612s		1626m		1626m	ν(CC)
1575w	1577m	1576m		1595m	1592s	1592s	1593s	ν(CC)
				1548w		1555w	1555w	ν_{int}(CC)
		1520s	1514w			1507s	1501w	$\nu_{as}(NO_2)$
1480m	1479m	1471m	1480w	1486w			1478w	ν(CC)
1446s	1448w	1450m		1458w				$\delta_{cp}(CH_2)$
		1420w	1424w	1433m			1418w	ν(CC)
1401s	1400w	1397m	1396w	1406w	1404m			ν(CC)(A-ring)
							1386m	ν(CC)
1345w	1343w							ν(CC)/δ(CH)
		1333s	1336s			1331s	1330s	$\nu_s(NO_2)/\nu$(CN)
1310w	1325ww			1312w				ν(CC)/δ(CH)
		1310sh	1305w			1310s	1312s	$\nu_s(NO_2)/\nu$(CN)
1295w	1292w		1282w					ν(CC)/δ(CH)/$\omega_{cp}(CH_2)$
1235w	1235m		1231w	1238w	1239s	1239m	1240s	ν(CC)/δ(CH)
1188m	1190w	1185m	1184w	1180m		1187m	1190m	δ(CH)
1153w	1150w	1154w	1156vw	1154w	1140w	1152w	1153s	δ(CH)
	1120vw	1125w	1123vw					δ(CH)
1108w	1110vw	1105vw		1107w				δ(CH)
1091w	1092vw			1093w		1088w	1091w	δ(CH)
		1072w	1072w	1067w	1064m			δ(CH)
1022w	1020m		1020w					δ(CH)/δ_{cp}(CH)
1000m		1004w	1005vw	1001w	997w			δ(CH)
954m		954w		959m	960vw	971vw	976vw	ρ(CH)
		933w						ρ(CH)
915w		910m	913vw	910w		909vw		ρ(CH)/$r_{cp}(CH_2)$
875vw		888w		890w	886vw		882m	ρ(CH)
860w								ρ(CH)/$r_{cp}(CH_2)$
	842w	840m		838vs	840vw	843s		ν_{sk}/ρ(CH)
		830sh	834w	820sh		822m		ρ(CH)
		803m	804vw		801w	797m	800w	ρ(CH)
789w	783vw	780m	780vw	780m	775vw			ρ(CH)
740vs	740m	740vs	747w	747s		756w	757vw	$r_{cp}(CH_2)$
695m		695vw		704s		701s		ν_{sk}/ρ(CH)
624w		635vw	632vw			632vw	635w	$\delta(NO_2)$
					590s			ν_{sk}
							574w	ν_{sk}
	540w	547w	552w	540w				ν_{sk}
					502vw		500vw	ν_{sk}
					456w			ν_{sk}
	418m				405s		417m	ν_{sk}
							359w	ν_{sk}

[a] Symbols refer to signal intensity, and the legend of symbols is as follows: vs, very strong; s, strong; m, medium; w, weak; vw, very weak; sh, shoulder. [b] Assignments deduced from the SERS results shown in this work. Symbols refer to vibrational modes, and legend of symbols is as follows: ν, stretching; δ, i.p. bending; t, twisting; ω, wagging; r, rocking; ρ, o.p. bending; s, symmetric; as, asymmetric; i.p., in-plane; o.p., out-of-plane; cp, cyclopentane ring of fluorene; sk, skeletal.

1000 cm^{-1} in fluorene are assigned to a deformation mode; however, the fact that this vibration decreased in the spectrum of the nitro compound makes it attributable to modes close to the nitro group; its weakening could be due to an anchorage effect imposed by the interaction between the O atoms of the nitro group and the adjacent H atom. The same can be said for the 2NF band at 1020 cm^{-1}. This behavior is also observed for the 2NF ρ(CH) bands at 954 and 695 cm^{-1}. On the other hand, the fact that three ρ(CH) bands at 933, 910, and 803 cm^{-1} are only observed in the spectrum of the nitro compound is due to the symmetry reduction in going from C_{2v} in fluorene to C_s in 2NF. Via a nitro substitution effect, some ρ(CH) bands remain at the same frequency, suggesting that they belong to vibrations far from the nitro group, probably from the unsubstituted benzene fragment. The weak fluorene IR bands at 633 and 624 cm^{-1} are assigned to aromatic δ(CCC) modes; the spectral shifting observed when going from fluorene to 2NF is due to the π electronic redistribution imposed by the nitro group. Similar behavior was observed for 1NP. In fact, the deep spectral changes observed in both the δ(CH) and ρ(CH) regions are due to the nitro substitution.

Bands belonging to the central pentacycle moiety in 2NF are easily ascribed, in comparison to anthracene and naphthalene; the main spectral differences should be ascribed to the pentacycle ring vibrations. IR bands in fluorene that appear at 1446, 1188, 1108, and 695 cm^{-1} are then assigned to the pentacycle ring and may be assigned to the CH_2 group and to the additional C−C bond existing in this compound.

In pyrene, there is a group of bands observed only in the IR spectra of this compound, appearing at 1559 and 1458 cm^{-1}, which have been assigned to the ν(CC) modes of bonds that belong to the center of the structure; this fragment is unique in these molecules of the series.

^{1}H NMR Spectra of Fluorene and 2-Nitrofluorene. ^{1}H NMR spectra of fluorene and 2NF (not shown) dissolved in acetone-d_6 show different group of signals between 8.6 and 7.3 ppm, corresponding to the aromatic protons, whereas the signal from the aliphatic protons appears near 4 ppm. Signals corre-

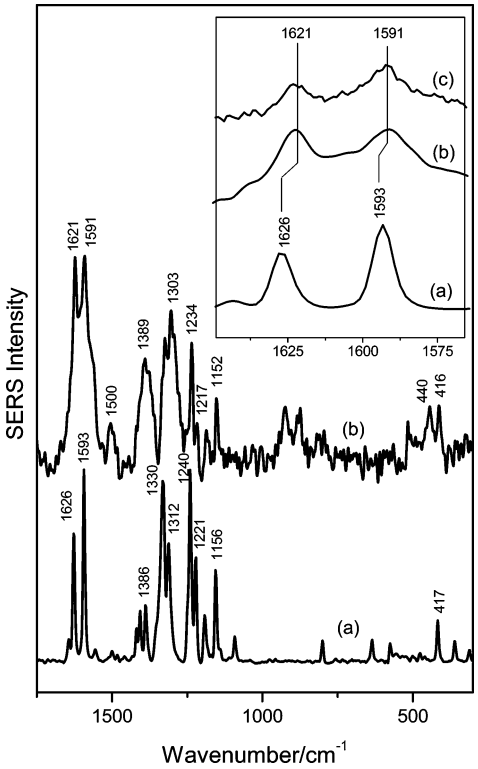

Figure 3. Raman and SERS spectra of 1NP (a) in solid (at 1064 nm) and (b) in silver borohydride (at 514.5 nm). Inset figure shows the following spectra in the 1700−1500 cm^{-1} range: (a) Raman spectrum of solid, (b) SERS spectrum on silver colloid borohydride at 514.5 nm, and (c) SERS spectrum on silver citrate at 785 nm.

sponding to the fluorene aromatic H atoms shift to a low field in the spectrum of 2NF. This result allowed us to propose that the NO_2 fragment is coplanar to the PAHs moiety in 2NF.

SEVS Study of the NPAH 1-Nitropyrene. *1. SERS of 1-Nitropyrene on Silver Colloids.* In Figure 3, the Raman spectrum of 1NP in the solid-state excited at 1064 nm is compared to the SERS spectrum of 1NP on a borohydride silver colloid excited at 514.5 nm. The reason for using the aforementioned laser lines can be explained as follows. The spectrum of the solid at 514.5 nm displays a strong fluorescence, overlapping the Raman signal, whereas the aforementioned silver colloid is not active at 1064 nm. On the other hand, we obtained the best results using this colloid, because the silver citrate colloid showed a low SERS intensity and strong bands due to citrate.

The most relevant spectral differences between the solid and the compound on borohydride silver colloid concern bands that are related to the nitro moiety and those belonging to the aromatic fragment close to the substitution site, in the region of 1700−1100 cm^{-1} (Figure 3). In fact, the $\nu_s(NO_2)/\nu(CN)$ bands that appear at 1330 and 1312 cm^{-1} in the solid shift to 1324 and 1303 cm^{-1} on the colloid. The relative intensity of these bands is inverted, observing a further enhancement of the band that appears at 1303 cm^{-1}, probably because of the higher contribution of the ν(CN) mode to this band. The weak band that is observed at 1500 cm^{-1} corresponds to the $\nu_{as}(NO_2)$ mode, which is enhanced in the SERS analysis, appearing with a medium intensity. The $\delta(NO_2)$ mode expected in the 650−600 cm^{-1} region is not observed in the SERS analysis. These changes clearly demonstrate the importance of the nitro group in regard to the interaction with the metal.

The two strong ν(CC) bands observed at 1627 and 1593 cm^{-1} display modifications of their relative intensities and frequencies upon adsorption onto silver. The first band increases its relative intensity and is shifted downward to 1621 cm^{-1}, whereas the second band only undergoes a slight shift downward.

To study the behavior of the CC stretching bands appearing at 1627 and 1593 cm^{-1} in more detail, in the inset figure of Figure 3, the SERS spectra of 1NP on two different silver colloids (citrate and borohydride) are compared to the Raman spectra of the solid in the aforementioned region. In the SERS spectrum recorded at 514.5 nm (on the silver borohydride colloid), a relative enhancement of the band at 1623 cm^{-1} is observed. In contrast, in the SERS recorded at 785 nm (on a citrate silver colloid), the relative intensity of these bands is similar to the solid spectrum. These phenomena are ascribed to resonant effects during excitation at 514.5 nm. The UV−visible spectra of the NPAHs display bands at <400 nm, in agreement with published data.[46] Therefore, the resonant effect must be associated with a metal-to-adsorbate charge-transfer mechanism.

The broad band that appears in the SERS spectrum at 1389 cm^{-1} is assigned to ν(CC) modes of the A-ring directly linked to the nitro group. Its significant enhancement in the SERS spectrum can be attributed to the proximity of this molecular moiety to the metal surface. In addition, bands corresponding to the aromatic rings between 1250 and 1200 cm^{-1}, which are due to ν(CC) coupled to δ(CH) modes, display a frequency shift by the surface effect, undergoing changes in the relative intensity, depending on the geometry of such vibrational modes. The broad bands that are observed in the 900−850 cm^{-1} region can be due to the borohydride oxidation products.

Finally, we have observed a new band at 444 cm^{-1} on the colloid, as well as a downward frequency shift of the band at 417 cm^{-1} by the surface effect; these bands are assigned to skeletal vibrations.

According to the SERS selection rules, the spectral profile of the adsorbate is strongly dependent on the orientation of the main molecular axes, with respect to the surface. In fact, those modes with a higher perpendicular polarizability component, with respect to the surface, will be enhanced the most.[47] Thus, SERS intensities provide valuable information about the molecular orientation that the adsorbate adopts once adsorbed on the metal surface.

The enhancement of in-plane ν(CC) modes reveals that 1NP is oriented perpendicularly, with respect to the metal surface, whereas the changes that occur in the nitro group indicate that the interaction occurs through the O atoms of the nitro moiety. The interaction induces a π electronic redistribution, primarily around both the nitro group and the aromatic portion in the vicinity of the substitution site. This interaction is very similar to that of nitrobenzene,[48] whose $\nu_s(NO_2)/\nu$(CN) band is shifted to lower frequencies upon adsorption onto a gold film through the O atoms. Assuming that the orientation of the molecule is rather perpendicular, as in the case of nitrobenzene, and considering that the asymmetric NO_2 stretching vibration is enhanced in the SERS spectrum, we suggest that the most probable orientation of 1NP on the silver surface is rather tilted, with the nitro group interacting with the metal through one O atom under a monodentate configuration (see Figure 4). This asymmetric interaction of 1NP with the surface may be induced by the steric hindrance of the B-ring, which is adjacent to the nitro group.

2. SERS of 1-Nitropyrene on Gold Surfaces. Previously, attempts to obtain the SERS spectrum of 1NP on gold colloids were performed at different excitation wavelengths. However, no SERS signal was obtained on colloids of this metal, probably because of a weaker affinity of this compound to this metal.

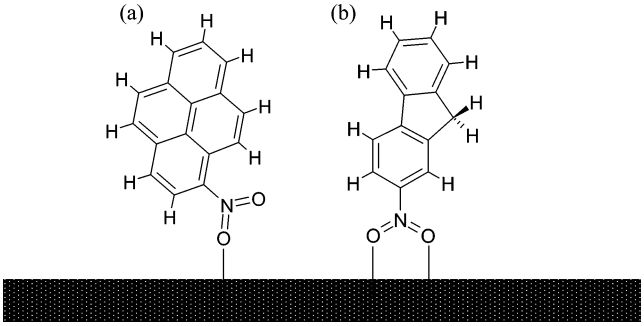

Figure 4. Adsorption mechanisms of (a) 1NP and (b) 2NF on the metal surfaces.

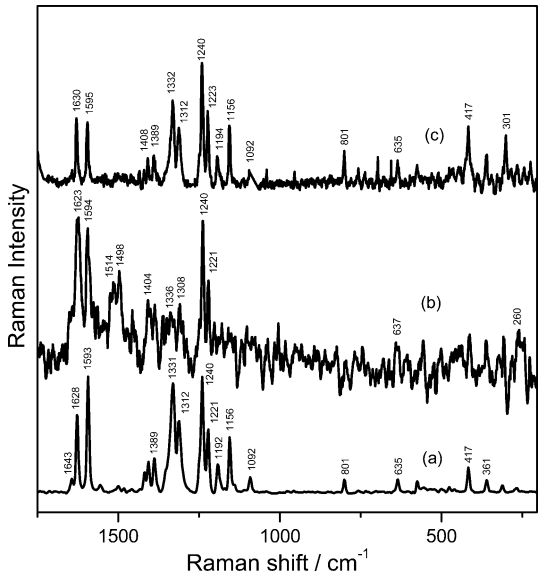

Figure 5. (a) Raman spectrum of 1NP in solid at 1064 nm. SERS spectra on a gold/germanium surface at (b) low and (c) high concentration. Excitation at 785 nm.

On the contrary, a SERS spectrum could be obtained on a gold/germanium film (Figure 5). Different SERS spectra were obtained by increasing the 1NP concentration on the surface; in Figure 5b and c, we display the SERS spectra corresponding to the lowest and highest concentrations, respectively. The highest concentration was obtained by adding several drops (ca. 100 μL) of the 1NP 10^{-5} M ethanol solution to the same area. The spectrum at high concentration (Figure 5c) is similar to that of the solid (Figure 5a), except for the relative intensity of the band that appears at 1595 cm^{-1}, which decreases by a surface effect, and the enhancement of the band at 301 cm^{-1}, which seems to be sensitive to the molecular organization on the surface. This fact indicates that, at the highest concentration, the adsorbate presents a multilayer-type organization on the metal surface. The spectrum at low concentration (Figure 5b) shows a different spectral pattern compared to that of the solid (Figure 5a), suggesting that it corresponds to the 1NP molecules that are directly attached to the metal. A remarkable change of the relative intensity of the symmetrical/asymmetrical NO_2 modes, but a lower frequency shift, are observed via the surface effect, in comparison to the SERS spectra observed on silver colloids. Although the interaction with the gold surface occurs through an O atom of the NO_2 group, this interaction seems to be weaker than that on silver surfaces, thus suggesting that the molecules are organized differently on both metals. In particular, the marked enhancement of the asymmetric NO_2 stretching mode on gold, in comparison to the symmetric stretching modes, indicates that the molecule is more tilted on this metal, in relation

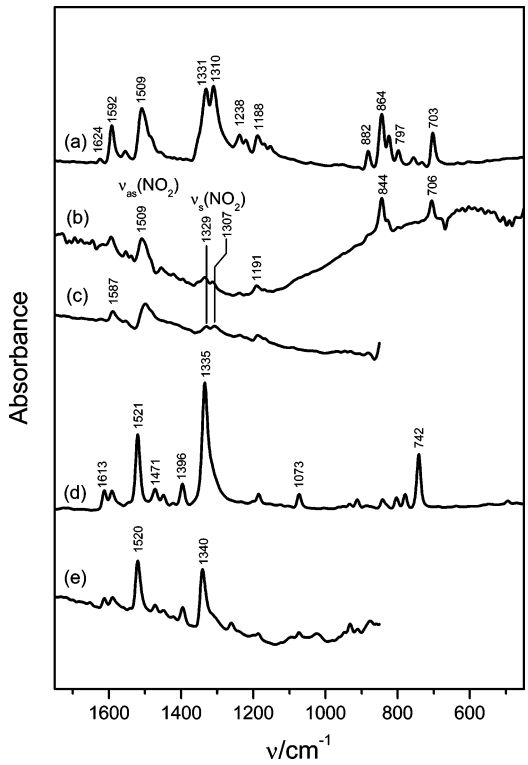

Figure 6. IR spectra of (a) 1NP and (d) 2NF. SEIR spectra of (b) 1NP on gold/germanium, (c) 1NP on Au/CaF_2, and (e) 2NF on Au/CaF_2.

to silver (see Figure 4), because, under such orientation, the symmetric modes tends to be parallel to the surface. The band observed at ~260 cm^{-1} in the spectrum of low concentration seems to correspond to the ν(Au−O) mode.

3. SEIR of 1-Nitropyrene on Gold Surfaces. Figure 6 shows the SEIR spectra of 1NP on gold/germanium (Figure 6b) and gold/CaF_2 films (Figure 6c), together with the IR spectrum in KBr (Figure 6a). The SEIR spectra show strong $\nu_{as}(NO_2)$ bands at 1509 cm^{-1} (on gold/germanium) and at 1499 cm^{-1} (on gold/CaF_2), whereas the corresponding $\nu_s(NO_2)/\nu$(CN) bands, at 1331 and 1310 cm^{-1}, are very much decreased (20%, in relation to the $\nu_{as}(NO_2)$ band). This result clearly supports the assumption that 1NP is adsorbed on the surface through a monodentate configuration, as it was also deduced from the SERS results. As mentioned previously, this adsorption mechanism is probably adopted because of the steric hindrance of the adjacent B-ring.

The band at 1624 cm^{-1}, which must correspond to a more symmetric ν(CC) mode of the A-ring, as deduced from its lower intensity in IR (Figure 6a), undergoes a slight intensity increase and downward shift, as a consequence of the proximity of this ring to the surface and its perpendicular orientation. In contrast, the mode at 1238 cm^{-1} undergoes a clear weakening, as in the case of the SERS. This leads us to assign this mode to ν(CC) modes far from the nitro group.

The gold/germanium film allowed us to study the SEIR region at <1000 cm^{-1}. The fact that two strong bands appear at 844 and 706 cm^{-1} suggests that they correspond to in-plane skeletal vibrations. On the other hand, the bands that appear at 882, 824, 797, and 755 cm^{-1} undergo a remarkable intensity decrease upon adsorption of the molecule on gold, thus indicating that they may correspond to out-of-plane CH vibrations.

SEVS Study of the NPAH 2-Nitrofluorene. *1. SERS of 2-Nitrofluorene.* Figure 7 displays the spectra of 2NF in the solid (Figure 7a) and that deposited on a gold/germanium surface at high (Figure 7b) and low (Figure 7c) concentrations, along

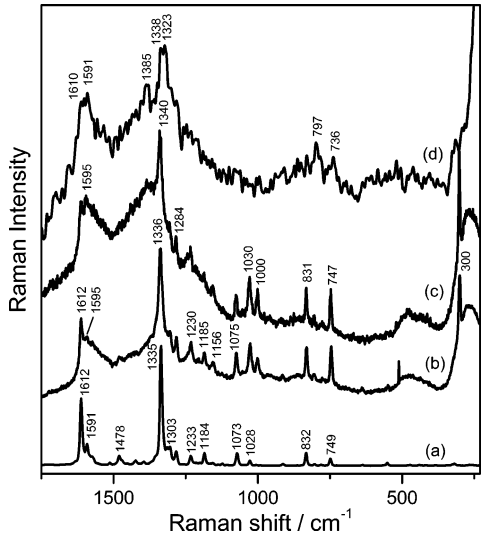

Figure 7. Raman and SERS spectra of 2NF (a) in solid, 1064 nm, (b) deposited on a gold/germanium surface at 785 nm, (c) after washing with ethanol, and (d) SERS spectrum on silver borohydride colloid at 514.5 nm.

with the spectrum of the compound on borohydride silver colloid (Figure 7d). The SERS spectrum of the sample on borohydride silver colloid shows a splitting of the $\nu_s(NO_2)/\nu(CN)$ band, observing two components at 1338 and 1323 cm^{-1}. The band at 1591 cm^{-1} in the solid is enhanced when the molecule is adsorbed on the colloid. In contrast to 1NP, the $\nu_{as}(NO_2)$ mode is not enhanced by a surface effect and the symmetric mode remains the strongest band in the SERS. Thus, the most probable interaction occurs through the NO_2 group, with the adsorbate oriented by a bidentate complex. This assumption is supported by the SEIR experiments (Figure 6). The bands that appear at 1030 and 1000 cm^{-1} are rather due to impurities that already exist in the gold surface.

We have observed the appearance of the band at ~270 cm^{-1} in the spectrum of the most diluted sample on the gold/germanium film, which could be attributed to the ν(Au−O) mode; this band was not clearly observed in the spectrum of the colloid, because of the existence of many oxygen-containing species in the medium.

Attempts to obtain a SERS spectrum with a low 1NF concentration on gold/germanium films, as in the case of 1NP, were done without success. We suggest that this is due to a weaker interaction of this molecule with gold films or to the fact that 1NF is partially photodegraded by the laser radiation when adsorbed onto the metal surface, as indicated by the appearance of two broad bands centered at 1390 and 1590 cm^{-1}.

However, we have tried to conduct an inverse experiment in which a highly concentrated sample was deposited on the gold/germanium film by adding several drops (ca. 100 μL) of the 2NF/ethanol solution (10^{-5} M) and then the resulting film was washed to attain a lower concentration onto the surface. The spectrum of the highest concentrated sample (Figure 7b) displays a similar pattern in relation to that of the solid (Figure 7a). When diluting the sample by washing (Figure 7c), we observed slight spectral changes, which suggested a surface effect: the enhancement of the band at ~1594 cm^{-1} and the shift of the symmetric NO_2 band from 1336 to 1340 cm^{-1}, which is also observed in the SEIR spectrum. These changes occur in the opposite direction, in relation to 1NP, and also support a different orientation of the NO_2 group in each 2NF.

2. SEIR of 1-Nitrofluorene. Spectra d and e in Figure 6 display the IR spectrum of 2NF in KBr and the SEIR of this molecule

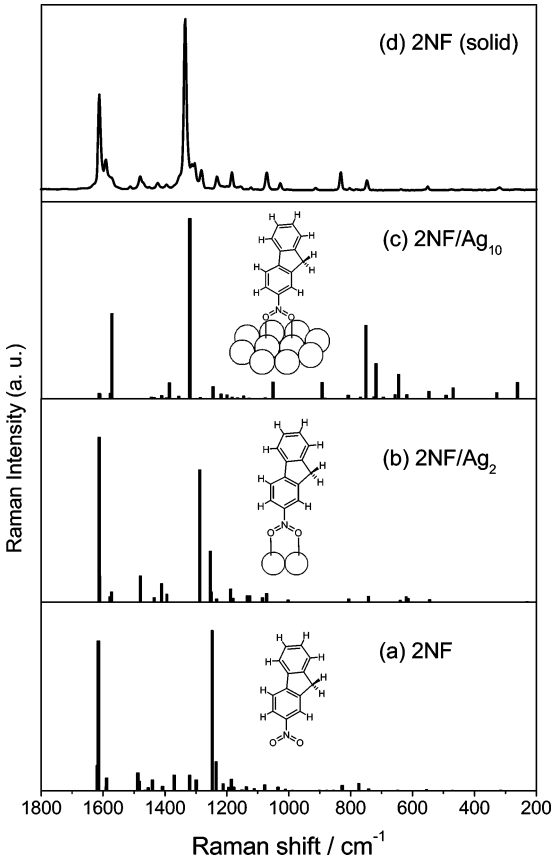

Figure 8. Calculated SERS spectra of (a) 2NF, (b) 2NF complex with 2 Ag atoms, and (c) 2NF complex with 10 Ag atoms. Panel d shows the Raman spectrum of solid 2NF.

on Au/CaF_2, respectively. The SEIR on gold/germanium film could not be obtained in this case. The SEIR spectrum of 2NF shows a different behavior of this molecule, in relation to 1NP. The band that appears at 1335 cm^{-1} that is due to $\nu_s(NO_2)/\nu$(CN) modes undergoes a moderate decrease and an upward shift to 1340 cm^{-1} but is still more intense than the corresponding $\nu_{as}(NO_2)$ band that appears at 1520 cm^{-1}, in contrast to that observed for 1NP. This effect is attributed to the different orientation and interaction mechanism of 2NF with the metal surface and is consistent with a rather bidentate interaction of 2NF with the surface, according to Figure 4. On the other hand, the difference in the shift of the $\nu_s(NO_2)/\nu$(CN) band can be also attributed to the bidentate configuration of the 2NF/Ag interaction, because a charge transfer from the π electronic system of the aromatic rings to the metal leads to an increase the double-bond character of the C−N bond. These results are consistent with the SERS spectrum of 2NF (see Figure 7). In fact, in the SERS spectrum, we also observed an upward shift of this band to 1340 (on gold film)/1338 cm^{-1} (on silver colloid) that is related to the bidentate interaction.

Theoretical SERS Spectra. Calculated Raman spectra were obtained for free 2NF and the complexes $2NF/Ag_2$ and $2NF/Ag_{10}$, supposing a perpendicular orientation of 2NF, with respect to the silver planar cluster, and a bidentate interaction of 2NF through both nitro O atoms. These spectra were compared to the Raman spectrum of the solid 2NF in Figure 8. To compare the theoretical frequencies with the experimental frequencies, we found that the scaling factor required to adjust both values was in the 0.953−0.963 range for the used basis set. In general, ν(CH) modes required a factor that is similar to the low limit of this range, whereas ν(CC) modes required a factor that is similar to the upper limit, so that it is possible to use an averaged

factor of 0.958 to reproduce most of the calculated frequencies. The calculated frequencies and intensities are shown in Figure 8.

The calculated spectra of 2NF in the presence of silver reveal that a significant electronic reorganization is occurring in the molecule upon interaction with the metal. In general, we have observed that the bands corresponding to the in-plane stretching modes at >1500 cm^{-1} shift downward, whereas those modes appearing below the latter wavenumber are shifted upward, thus indicating that the interaction with the metal induces a higher electronic delocalization in the aromatic rings. This tendency is gradual, observing a progressive shift in the aforementioned indicated directions in the following sense: 2NF < 2NF/Ag_2 < 2NF/Ag_{10}.

The bands at 1615/1580 cm^{-1} undergo both a downward shift and an inversion in going from the free molecule to the 2NF/Ag_{10} complex. The lower component appears in the latter complex at 1570 cm^{-1}, whereas the higher component undergoes a much weaker shift to 1612 cm^{-1}. According to our calculations, the lower band is assigned to the A-benzene ring, which is, thus, the ring directly attached to the NO_2 group. In the SERS spectra (Figure 7), we observed an inversion of the 1612/1591 cm^{-1} bands, similar to that observed in the calculated spectrum of 2NF.

The enhancement of the 2NF bands at 1316, 750, and 716 cm^{-1}, which are attributed to the 2NF A-ring, is also a consequence of the interaction of the nitro group with the metal.

The $\nu_s(NO_2)/\nu(CN)$ vibrations contribute to several vibrations in the 1300−1400 cm^{-1} region. In all cases, we have observed a shift upward to 1380 cm^{-1}, as a consequence of the interaction with the metal. This change suggests a bidentate interaction of 2NF with the metal through the NO_2 group, in good agreement with the results found by SERS and SEIR. In addition, the enhancement of the $\delta(NO_2)$ band at 644 cm^{-1} in the theoretical spectra is a consequence of the interaction of the nitro group with the metal.

The calculations also allowed the identification of the normal modes related to the new bonds established in the metal/2NF interaction. The calculation of several modes at <300 cm^{-1}, which involve ν(Ag−O) vibrations, confirms that the NPAH molecules could be chemisorbed onto the metal surface through the O atoms.

The general agreement between the experimental and theoretical results further support the orientation and interaction mechanism proposed for this molecule on the metal surface.

Conclusions

The nitro polyacyclic aromatic hydrocarbons (NPAHs)−metal surface interaction is verified through the NO_2 fragment, adopting a preferential perpendicular orientation onto the surface in the molecular systems. The interaction mechanism and the strength of the interaction are different for 1-nitropyrene (1NP) and 2-nitrofluorene (2NF), mainly because of the different structure of the molecules. Both molecules display a different affinity toward the metal surfaces used in this work; 1NP is adsorbed to the surface through a monodentate complexation, whereas 2NF interacts with the substrate with both O atoms through a bidentate interaction. The different interaction mechanisms lead to differences in the relative enhancement of $\nu_{as}(NO_2)/\nu_s(NO_2)$ bands and the position of these bands at those corresponding to the benzene rings directly attached to the nitro group. The chemical interaction of the molecule with the metal was deduced from the changes observed in the NPAHs bands upon adsorption on the surface. This chemisorption could lead to a charge transfer between the adsorbate and the metal, as evidenced by the changes observed in the Raman spectra at different excitation wavelengths.

Among the different metal surfaces used in this work, the most-intense SERS spectra were obtained for borohydride silver colloid in macro Raman experiments. No SERS signal was detected on gold colloids, probably because of the lower affinity of NPAHs for this metal. However, the surface-enhanced Raman scattering (SERS) and surface-enhanced infrared (SEIR) intensity and sensitivity was higher for the SEVS experiments that were performed for the gold films.

These results demonstrated that, for the studied NPAHs, a certain chemical interaction (chemisorption) with the metal used is necessary to observe any surface-enhanced vibrational spectroscopy (SEVS) spectrum. This fact explains why neither SERS nor SEIR spectra were observed for the parent PAHs molecules, where no attaching group exists in the molecular structure.

Density functional theory calculated frequencies and intensities predict an electronic reorganization of the 2NF molecular systems upon interaction with the metal. The agreement between SERS and SEIR spectra and the calculated spectra was significant, thus confirming the perpendicular orientation and the bidentate interaction that is supposed for the interaction of 2NF with the modeled metal surface.

Acknowledgment. The authors acknowledge Project Fondecyt 1010867 from Conicyt (Chile), Convenio Conicyt/CSIC 2001/2002, and Grant No. BFM/2265/2001 from Dirección General de Investigación, Ministerio de Ciencia y Tecnología (Spain) for financial support.

References and Notes

(1) Nitrogenated Polycyclic Aromatic Hydrocarbons, Environmental Health Criteria No. 229, World Health Organization, in preparation. (Available via the Internet at http://www.who.int/pcs/pubs/pub_ehc_alph.htm.)

(2) Schmidt, W. *Polycyclic Aromatic Hydrocarbons and Astrophysics*; D. Reidel Publishing Company: Dordrecht, The Netherlands, 1987; pp 149−164.

(3) Busch, H. *The Molecular Biology of Cancer*; Academic Press: New York, 1974.

(4) Bartle, K. D.; Lee, M. L.; Wise, S. A. *Chem. Soc. Rev.* **1981**, *10*, 213.

(5) Ebert, L. B. *Polynuclear Aromatic Hydrocarbons*; ACS Symposium Series 217; American Chemical Society: Washington, DC, 1988.

(6) Ritter, C. L.; Culp, S. J.; Freeman, J. P.; Marques, M. M.; Beland, F. A.; Malejka-Giganti, D. *Chem. Res. Toxicol*. **2002**, *15*, 536.

(7) Li, D.; Wang, M.; Firozi, P. F.; Chang, P.; Zhang, W.; Baer-Dubowska, W.; Moorthy, B.; Vulimiri, S. V.; Goth-Goldstein, R.; Weyand, E. H.; DiGiovanni, J. *Environ. Mol. Mutagen*. **2002**, *39*, 193.

(8) Bacolod, M. D.; Basu, A. K. *Mutagenesis* **2001**, *16*, 461.

(9) El-Bayoumy, K.; Johnson, B. E.; Roy, A. K.; Upadhyaya, P.; Partian, S. J.; Hecht, S.-S. *Environ. Health Perspect.* **1994**, *102*, 31.

(10) Li, P. P. F.; Church, J. S. *J. Mol. Struct.* **2000**, *217*, 550.

(11) Landhoff, S. R.; Bauschlicher, C. W., Jr.; Hudgins, D. M.; Sandford, S. A.; Allamandola, A. J. *J. Phys. Chem*. **1998**, *102*, 1632.

(12) Hudgins, D. M.; Sandford, S. A.; Allamandola, L. J. *J. Phys. Chem*. **1994**, *98*, 4243.

(13) Hudgins, D. M.; Allamandola, L. J. *J. Phys. Chem*. **1995**, *99*, 3033.

(14) Hudgins, D. M.; Allamandola, L. J. *J. Phys. Chem.* **1995**, *99*, 8978.

(15) Witteborn, F. C.; Sandford, S. A.; Bregman, J. D.; Allamandola, L. J.; Cohen, M.; Wooden, D. *Astrophys. J.* **1989**, *341*, 270.

(16) Flickinger, G. C.; Wdwiak, T. J. *Astrophys. J.* **1990**, *362*, L71.

(17) Cyvin, B. N.; Cyvin, S. J. *Spectrosc. Lett*. **1986**, *19*, 1161.

(18) Juchnovski, N.; Andreev, G. N. *Bulg. Acad. Sci.* **1983**, *16*, 389.

(19) Trotter, J. *Acta Crystallogr*. **1959**, *12*, 237.

(20) Fleischmann, M.; Hendra, P. J.; McQuillan, A. J. *Chem. Phys. Lett*. **1974**, *26*, 163.

(21) Harstein, A.; Kirtley, J. R.; Tsang, J. C. *Phys. Rev. Lett*. **1980**, *45*, 201.

(22) Osawa, M.; Ikeda, M. *J. Phys. Chem*. **1991**, *95*, 9914.

(23) Burstein, E.; Chen, B. J.; Chen, C. Y.; Lundquist, S.; Tosatti, E. *Solid State Commun.* **1979**, *29*, 567.

(24) Campos-Vallette, M.; Diaz, G.; Clavijo, R. E.; Martinez, Y.; Mendizabal, F.; Costamagna, J.; Canales, J. C.; García-Ramos, J. V.; Sanchez-Cortes, S. *Vib. Spectrosc.* **2001**, *27*, 15.
(25) Johnson, E.; Aroca, R. *J. Phys. Chem*. **1995**, *99*, 9325.
(26) Van Duyne, R. P.; Hulteen, J. C.; Treichel, D. A. *J. Chem. Phys*. **1993**, *99*, 2101.
(27) Vo-Dinh, T.; Fetzer, J.; Campiglia, A. D. *Talanta* **1998**, *47*, 943 and references therein.
(28) Vo-Dinh, T. *TrAC, Trends Anal. Chem.* **1998**, *17*, 557.
(29) Enlow, P. D.; Buncick, M.; Warmarck, R. J.; Vo-Dinh, T. *Anal. Chem*. **1986**, *58*, 1119.
(30) Scott, A. P.; Radom, L. *J. Phys. Chem*. **1996**, *100*, 16502.
(31) Wong, M. W. *Chem. Phys. Lett*. **1996**, 256.
(32) Lee, P. C.; Meisel, D. *J. Phys. Chem*. **1982**, *86*, 3391.
(33) Creighton, J. A.; Blatchford, C. G.; Albrecht, M. G. *J. Chem. Soc., Faraday Trans. 2* **1979**, *75*, 790.
(34) Domingo, C.; Sanchez-Cortes, S.; Garcia-Ramos, J. V.; Aznarez, J. A. *Langmuir* **2001**, *17*, 1157.
(35) Slater, J. C. *Quantum Theory of Molecular and Solids*; McGraw−Hill: New York, 1974; Vol. 4.
(36) Vosko, S. H.; Wilk, L.; Nusair, M. *Can. J. Phys.* **1980**, *58*, 1200.
(37) Dunning, T. H., Jr.; Hay, P. J. In *Modern Theoretical Chemistry*; H. F. Schaefer, III, Ed.; Plenum: New York, 1977; Vol. 3, pp 1−27.
(38) Frisch, M. J.; Trucks, G. W.; Schlegel, H. B.; Scuseria, G. E.; Robb, M. A.; Cheeseman, J. R.; Zakrzewski, V. G.; Montgomery, J. A., Jr.; Stratmann, R. E.; Burant, J. C.; Dapprich, S.; Millam, J. M.; Daniels, A. D.; Kudin, K. N.; Strain, M. C.; Farkas, O.; Tomasi, J.; Barone, V.; Cossi, M.; Cammi, R.; Mennucci, B.; Pomelli, C.; Adamo, C.; Clifford, S.; Ochterski, J.; Petersson, G. A.; Ayala, P. Y.; Cui, Q.; Morokuma, K.; Malick, D. K.; Rabuck, A. D.; Raghavachari, K.; Foresman, J. B.; Cioslowski, J.; Ortiz, J. V.; Baboul, A. G.; Stefanov, B. B.; Liu, G.; Liashenko, A.; Piskorz, P.; Komaromi, I.; Gomperts, R.; Martin, R. L.; Fox, D. J.; Keith, T.; Al-Laham, M. A.; Peng, C. Y.; Nanayakkara, A.; Gonzalez, C.; Challacombe, M.; Gill, P. M. W.; Johnson, B. G.; Chen, W.; Wong, M. W.; Andres, J. L.; Head-Gordon, M.; Replogle, E. S.; Pople, J. A. *Gaussian 98*, revision x.x; Gaussian, Inc.: Pittsburgh, PA, 1998.
(39) Lin-Vien, D.; Colthup, N. B.; Fately; W. G.; Grasselli, J. G. *The Handbook of Infrared and Raman Characteristic Frequencies of Organic Molecules*, 1st ed.; Academic Press: Boston, 1991.
(40) Nakamoto, K. *Infrared and Raman Spectra of Inorganic and Coordination Compounds*, 5th ed.; Wiley−Interscience: London, 1997.
(41) Socrates, G. *Infrared Characteristic Group Frequencies*; Wiley: New York, 1980.
(42) Passingham, C.; Hendra, P. J.; Hodges, C.; Willis, H. A. *Spectrochim. Acta, Part A* **1991**, *47A*, 1235.
(43) Maddams, W. F. G.; Royaud, I. A. M. *Spectrochim. Acta, Part A* **1990**, *46A*, 309.
(44) Figueroa, K.; Campos-Vallette, M.; Contreras, R. *Z. Naturforsch. A: Phys. Sci.* **1990**, *45A*, 1199.
(45) Figueroa, K.; Campos-Vallette, M.; Rey-Lafon, M. *Spectrochim. Acta, Part A* **1990**, *46A*, 1659.
(46) Karcher, W.; Fordham, R. J.; Dubois, J. J.; Glaude, P. G. J. M.; Ligthart, J. A. M. *Spectral Atlas of Polycyclic Aromatic Compounds*; D. Reidel Publishing Company: Dordrecht, The Netherlands, 1985.
(47) Moskovits, M. *Rev. Mod. Phys*. **1985**, *57*, 783.
(48) Gao, P.; Weaver, M. J. *J. Phys. Chem.* **1985**, *89*, 5040.